Prediction and analysis of a sodium ion electrolyte: $Li_2Na_2P_2S_6$

Yan Li[1], Zachary D. Hood[2] and Natalie A. W. Holzwarth[1]

[1]Department of Physics, Wake Forest University, Winston-Salem, NC 27109, USA

[2]Electrochemical Materials Laboratory, MIT, Cambridge, MA 02139, USA

Acknowledgements: *This work is supported by NSF grant DMR-1507942. Computations were performed on the Wake Forest University DEAC cluster, a centrally managed resource with support provided in part by the University.*

Outline

Three focuses of submitted work "***Computational and experimental (re)investigation of the structural and electrolyte properties of $Li_4P_2S_6$, $Na_4P_2S_6$, and $Li_2Na_2P_2S_6$***" by Yan Li, Zachary D. Hood, and N. A. W. Holzwarth,

- ❑ **Crystal structure stabilities of $Li_4P_2S_6$ and $Na_4P_2S_6$**

The Helmholtz free energy:

$$F(T) = F_{SL}(T) + F_{vib}(T) = U_{SL} + F_{vib}(T)$$

$$F_{vib}(T) = k_B T \int_0^\infty d\omega \ln\left(2\sinh\left(\frac{\hbar\omega}{2k_B T}\right)\right) g(\omega)$$

Ground state structure:

$Na_4P_2S_6$: Monoclinic **C2/m** (#12)

$Li_4P_2S_6$: Hexagonal **P$\bar{3}$m1** (#164)

consistent with those experiment results[1-3]

See more at http://users.wfu.edu/natalie/presentations/

This talk:

- ❑ **Structure and stability of predicted mixed ion electrolyte $Li_2Na_2P_2S_6$**
- ❑ **Performance of $Li_2Na_2P_2S_6$ in comparison with $Na_4P_2S_6$ as solid electrolytes**

[1]Neuberger et al., *Dalton Trans.* **47**, 11691-11695 (2018)
[2]Kuhn et al., *Z. Anorg. Allg. Chem.* **640**, 689-692 (2014)
[3]Hood et al., Manuscript in preparation.

03/02/2020 March 2020 APS 1

My talk is based on our recently submitted work "***Computational and experimental (re)investigation of the structural and electrolyte properties of $Li_4P_2S_6$, $Na_4P_2S_6$, and $Li_2Na_2P_2S_6$***" which has three main focuses. In the first part of the work, we showed that the enhanced computational methods with consideration of phonon contributions can explain the experimentally observed structures of $Na_4P_2S_6$ and its $Li_4P_2S_6$ analog.

Studies on these two materials also prompt an investigation of their alloys, one of them has composition $Li_2Na_2P_2S_6$. The following slides will show the predicted structures of this mixed ion material and the stability analysis in terms of reaction energies of proposed reaction pathways. Also the electrolyte properties of $Li_2Na_2P_2S_6$ will be discussed in comparison with those of $Na_4P_2S_6$.

Summary of computational methods

- Density Functional Theory (DFT) and Density Functional Perturbation Theory (DFPT) with the modified Perdew-Burke-Ernzerhof generalized gradient approximation[1] **(PBEsol GGA)**
- The projector augmented wave (PAW) formalism using ABINIT (https://www.abinit.org) & QUANTUM ESPRESSO (http://www.quantum-espresso.org)
- Datasets generated by ATOMPAW code available at http://pwpaw.wfu.edu
- Visualization software: XCrySDen, VESTA
- Space-group analysis: FINDSYM
- X-ray powder diffraction: Mercury

[1]Perdew et al., *Phys. Rev. L.* **100**, 136406 (2008)

The computational methods are based on Density Functional Theory (DFT) and Density Functional Perturbation Theory (DFPT) using the Projector Augmented Wave (PAW) formalism. The PAW basis and projector functions were generated by the ATOMPAW code and used in both the ABINIT and QUANTUM ESPRESSO packages. In the present work, the PBEsol GGA was used to treat the exchange and correlation effects.

The prototypic structure

$Na_4P_2S_6$ crystallizes in a base-centered monoclinic structure with space group C2/m (#12)[1,2] and this material was also found to have appreciable Na ion conductivity ($3x10^{-6}$ S/cm) at room temperature[2].

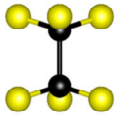

$(P_2S_6)^{4-}$ units with D_{3d} symmetry

g-type Na

h-type Na

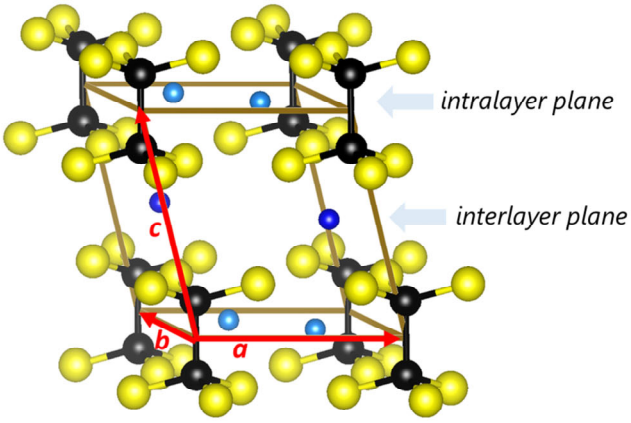

Primitive cell with 12 atoms/formula unit

[1]Kuhn et al., *Z. Anorg. Allg. Chem.* **640**, 689-692 (2014)
[2]Hood et al., Manuscript in preparation.

This diagram shows the ball and stick model of the C2/m structure in primitive cell setting, in which the P_2S_6 building blocks aligned orderly and uniformly throughout the space. Such structural framework may benefit the diffusions of Na ions in the material.

As what we see this structure has two crystallographically distinct Na sites with Wyckoff labels g and h, respectively. Each g-type Na ion is located in an intralayer plane which contains the P_2S_6 units, while each h site Na ion is located in an interlayer plane between the P_2S_6 units. Staring with the monoclinic structure of the pure Na material, we predicted the possible structures of the mixed ion material $Li_2Na_2P_2S_6$ based on the idea of ionic substitution.

Structures of the predicted material: $Li_2Na_2P_2S_6$

Replace the (a) *g*-type or (b) *h*-type Na ions in the monoclinic $Na_4P_2S_6$ with Li ions

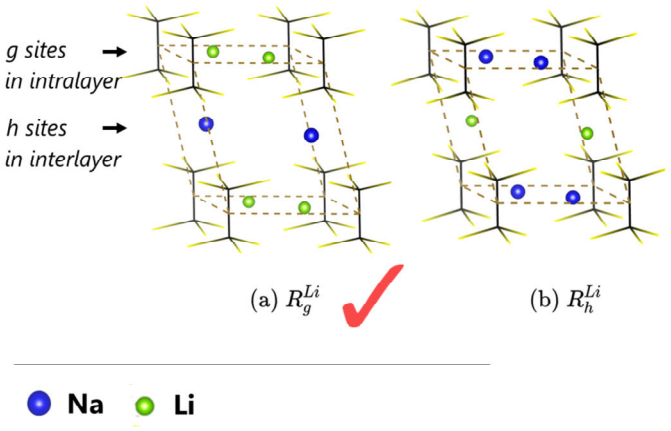

TABLE: Comparison of the optimized lattice parameters for $Li_2Na_2P_2S_6$ in the R_g^{Li} and R_h^{Li} structures. Also listed is the static lattice energy differences U_{SL} referenced to the energy of the R_h^{Li} structure in units of eV/formula unit.

		R_g^{Li}	R_h^{Li}
Primitive cell:	$a = b$ (Å)	6.18	6.46
	c (Å)	7.50	7.01
	$\alpha = \beta$ (deg)	97.77	97.88
	γ (deg)	119.21	118.43
Conventional cell:	a_c (Å)	6.26	6.61
	b_c (Å)	10.67	11.10
	c_c (Å)	7.50	7.01
	β_c (deg)	105.50	105.54
	ΔU_{SL} (eV/FU)	-0.16	0.00

The left diagram illustrates one likely geometry R_g^{Li} of atomic arrangements, generated by replacing all equivalent Na ions at g sites with Li ions. And by substituting the Li ions for all h-type Na ions in interlayer planes, we obtain another possible atomic configuration R_h^{Li}.

After optimization, we found both proposed structures retain their space group symmetry C2/m. For the reason that R_g^{Li} results in a lower static energy structure relative to R_h^{Li}, the configuration R_g^{Li} is determined to be the ground state structure of $Li_2Na_2P_2S_6$ and will be used in subsequent analysis and simulations.

Comparison of phonon spectra

$Na_4P_2S_6$ in the C2/m Structure (36 modes)

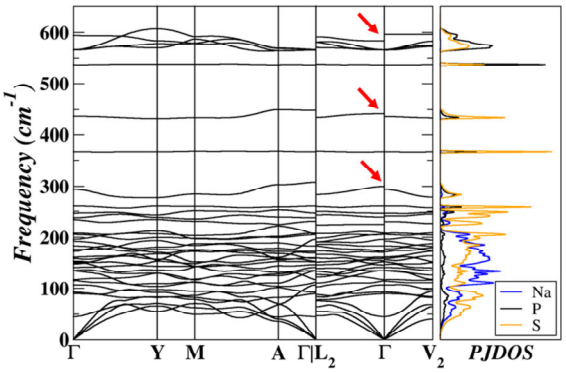

Na^+ 0~300 cm^{-1}

$(P_2S_6)^{4-}$ 300~600 cm^{-1}

$Li_2Na_2P_2S_6$ in the C2/m Structure (36 modes)

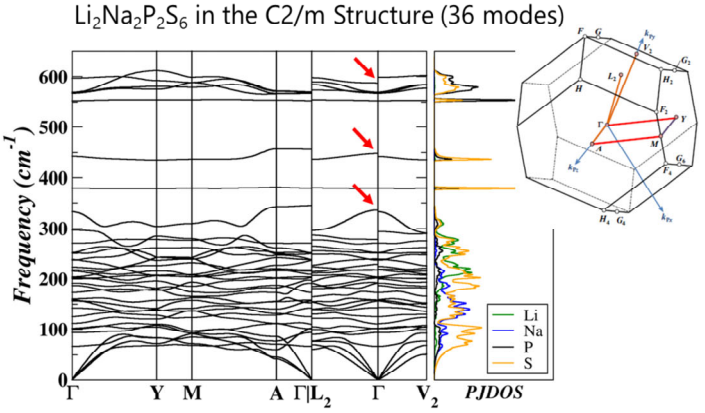

Li^+ 0~320 cm^{-1} evidence of dynamical stability

[1]Suggested path: Hinuma et al., *Comp. Mat. Sci.* **128**, 140-184 (2017)
[2]Li et al., *J. Phys. Condens. Matter,* **32**, 055402 (2019)

PJDOS: $g^a(\omega) \equiv \frac{V}{(2\pi)^3}\int d^3q \sum_{\nu=1}^{3N}(\delta(\omega-\omega_\nu(\mathbf{q}))W_a^\nu(\mathbf{q}))$

Discontinuous branches at Γ: coupling between photon and photon[2]

Here we see that phonon dispersion curves of the two materials are very similar with the same number of modes covering an almost identical range of frequencies. For the case of $Li_2Na_2P_2S_6$, the fact of having all real phonon frequencies implies that its possible ground state structure is dynamically stable.

As highlighted by short red arrows, there are several branches that are not continuous functions of q near gamma point. The physical reason for this kind of discontinuity is explained in terms of the coupling between the optical phonon modes and the electromagnetic field. For some of you who interest in such coupling effects, detailed discussions can be found in our published paper "Li et al., *J. Phys. Condens. Matter,* 32, 055402 (2019)".

Stability of the predicted material: $Li_2Na_2P_2S_6$

The possible reaction pathway:

$$Na_4P_2S_6 + 2\,Li \rightarrow Li_2Na_2P_2S_6 + 2\,Na$$

$$\Delta F(T) = \Delta U_{SL} + \Delta F_{vib}(T) + \Delta F_{\text{elec}}^{\text{metal}}(T)$$

trivial contribution (10^{-3} eV)

$$\Delta = \Delta^{Products} - \Delta^{Reactants}$$

Energy changes at T = 300 K in eV:

$$\Delta U_{SL} = -0.29$$
$$\Delta F_{vib} = -0.06$$
$$\Rightarrow \quad \Delta F = -0.35$$

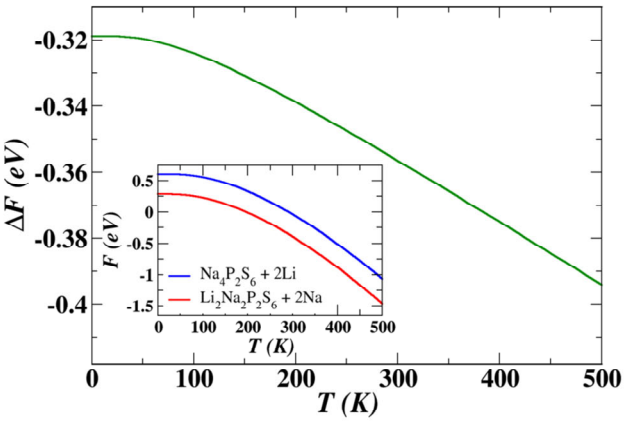

Negative energies (net released energies) implies that the products $Li_2Na_2P_2S_6$ + 2 Na is stable with respect to the reactants $Na_4P_2S_6$ + 2 Li.

03/02/2020 March 2020 APS 6

To further evaluate the stability of this predicted alloyed material $Li_2Na_2P_2S_6$, we proposed this possible reaction pathway and calculated the reaction energy which is determined from the energy difference between the right side products and the left-side reactants. For each component, the energy of it is obtained from the sum of static and vibrational contributions. In particular for Li and Na in their metallic form, we also considered the energy due to the temperature-dependent excitations, but it turns out this contribution is very small compared to others and can be neglected.

It shows that at room temperature, the reaction energy is -0.35 eV. The figure on the right demonstrates that the reaction energy is gradually decreasing along with the increasing temperature, suggesting that it is energetically favorable for Li to replace Na according to this reaction over a significant temperature range.

More possible reaction pathways

TABLE: Computed energy differences for indicated reactions in eV units, evaluated at T = 300 K and neglecting electronic excitation contributions.

No.	Reaction: $R \rightarrow P$	ΔU_{SL}	ΔF_{vib}	ΔF
1	$Na_4P_2S_6 + 2\ Li \rightarrow Li_2Na_2P_2S_6 + 2\ Na$	-0.29	-0.06	-0.35
2	$2\ Li + 2\ Na + 2\ P^{a} + 6\ S^{b} \rightarrow Li_2Na_2P_2S_6$	-10.62	0.06	-10.56
3	$\frac{1}{2}\ Na_4P_2S_6 + \frac{1}{2}\ Li_4P_2S_6 \rightarrow Li_2Na_2P_2S_6$	0.13	-0.03	0.10
4	$\frac{1}{2}\ Na_4P_2S_6 + \frac{1}{2}\ Li_3PS_4{}^{c} + \frac{1}{12}\ P_4S_4{}^{d} \rightarrow Li_2Na_2P_2S_6$	-0.24	-0.02	-0.26
5	$Na_3PS_4{}^{e} + Li_3PS_4{}^{c} + \frac{1}{6}\ P_4S_4{}^{d} \rightarrow Li_2Na_2P_2S_6$	-0.48	-0.00	-0.48
6	$Na_3PS_4{}^{e} + \frac{1}{3}\ P_4S_{10}{}^{f} + 2\ Li \rightarrow Li_2Na_2P_2S_6$	-5.01	0.06	-4.95
7	$Li_3PS_4{}^{c} + \frac{1}{3}\ P_4S_{10}{}^{f} + 2\ Na \rightarrow Li_2Na_2P_2S_6$	-4.70	0.07	-4.63

[a] Black phosphorous with Space Group *Cmce* (#64); from Brown et al. *Acta Cryst.* **19**, 684 (1965).
[b] Orthorhombic (α-S8) with Space Group *Fddd* (#70); from S. J. Rettig and J. Trotter, *Acta Cryst. C* **43**, 2260 (1987).
[c] γ-Li3PS4 with Space Group $Pmn2_1$ (#31); from Homma et al., *Solid State Ionics* **182**, 53 (2011).
[d] α-P4S4 with Space Group *C2/c* (#15); from Minshall et al., *Acta Cryst. B* **34**, 1326 (1978)..
[e] α-Na3PS4 with Space Group $P42_1c$ (#114); from Jansen et al., *J. Solid State Chem.* **99**, 110 (1992).
[f] P_4S_{10} with Space Group $P\bar{1}$ (#2); from Vos et al., *Acta Cryst.* **19**, 864 (1965).

Besides the possible synthesis route given in the previous slide, there are a number of other possible reactions we can imagine to produce the mixed ion electrolyte $Li_2Na_2P_2S_6$. In this table, we summarized the room-temperature reaction energies for some of those pathways. Here we see that the only reaction that has a positive reaction energy ΔF is reaction No. 3, which means the mixed material is unstable relative to these two left-side reactants. But we also learn from the experiment that the pure Li material $Li_4P_2S_6$ forms at very high temperatures, which implies that it is still possible to produce $Li_2Na_2P_2S_6$ via a low-temperature synthesis process with the metal-stable phase of $Li_4P_2S_6$ as one of the reactants.

Ion migration of vacancy mechanisms

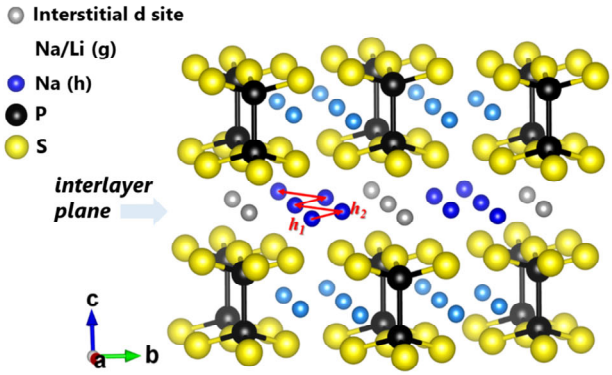

Activation energy: $E_a = E_m^{NEB} + \frac{1}{2}E_f$

Nudged Elastic Band[1] algorithm ⟹ E_m^{NEB}

$E_{defect}(Nah - Nad) - E_{perfect}$ ⟹ E_f

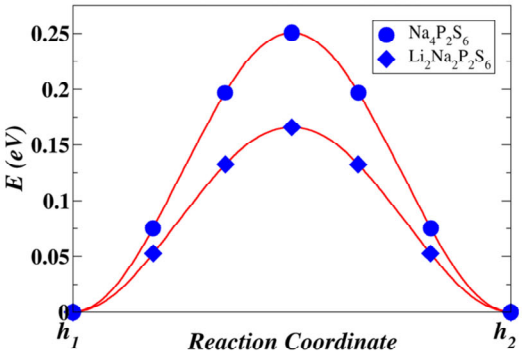

Configuration energy diagram results of NEB calculation of Na ion vacancy migration along one step of the indicated pathway.

[1]Henkelman et al., *J. Chem. Phys.* **113**, 9901-9904 (2000)

To understand the conductivity properties of the mixed ion material $Li_2Na_2P_2S_6$ in comparison with the pure Na material $Na_4P_2S_6$, we investigated the diffusion mechanisms and estimated the related activation energy E_a for Na ions hopping for both materials. And among many possible migrating paths, we identified that the most favorable path for Na ion vacancy migration appears to be between h sites. When viewing down the c axis, we would see the hops from one host h site to the adjacent vacancy construct a continuous zig-zag path from one side of the crystal structure to another. The resulted NEB diagram between such two local minimum energy configurations shows that the energy barrier of the mixed material is lower by about 0.1 eV than of the pure Na material.

Within this methodology, the activation energy E_a of the perfect crystal includes both migration energy E_m and also the formation energy E_f which is associated with the creation of a vacancy-interstitial pair (defect). In this diagram, the extra gray balls represent the interstitial d sites from which the defect formation energy E_f is determined.

Migration study using molecular dynamics simulations

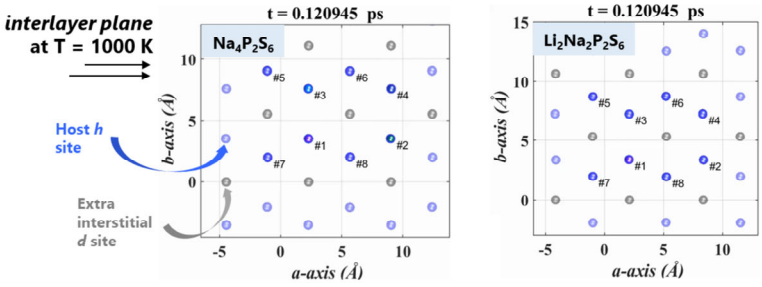

$$C^s_{h\leftrightarrow h}(t) = \begin{cases} C^s_{h\leftrightarrow h}(t-\Delta t) & \text{No config. change} \\ C^s_{h\leftrightarrow h}(t-\Delta t)+1 & h \leftrightarrow \text{nn } h \end{cases}$$

$$C^s_{h\leftrightarrow d}(t) = \begin{cases} C^s_{h\leftrightarrow d}(t-\Delta t) & \text{No config. change} \\ C^s_{h\leftrightarrow d}(t-\Delta t)+1 & \{h,d\} \leftrightarrow \text{nn } \{d,h\} \end{cases}$$

with $C^s_{h\leftrightarrow h}(t=0) = 0 = C^s_{h\leftrightarrow d}(t=0)$.

$$H_{h\leftrightarrow h}(t) = \frac{1}{16}\sum_{s=1}^{16} C^s_{h\leftrightarrow h}(t)$$

$$H_{h\leftrightarrow d}(t) = \frac{1}{16}\sum_{s=1}^{16} C^s_{h\leftrightarrow d}(t).$$

- No g → h and g → g hopping
- All migrations occur within interlayer plane containing h-type Na ions
- Direct h → h vacancy migration is consistent with NEB analysis
- Indirect h → d → h vacancy migration is prevalent
- No interstitial d → d migration

Both Na ion vacancy sites and indirect participation of interstitial sites contribute to the conductivity throughout the interlayer plane

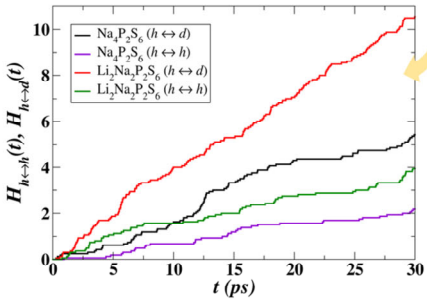

**AIMD simulations were carried out using supercells composed of 2x1x2 conventional units (96 atoms)*

By directly observing the trajectories of atoms produced by molecular dynamics simulations, we found that for both materials all migration events only occur within the interlayer plane containing all h sites. Here we have movies for visualizing the trajectories of h-type Na ions at T = 1000K. At the beginning of the calculation, there are 8 Na ions resided at each interlayer plane in the simulation cell. More balls were placed to display that the Na ion may migrate to the neighboring cells.

Note in this document, the animations were represented by the superposed snapshots of the ion positions at t =~10 ps, ~15 ps and ~30 ps as presented in the next 3 slides.

Migration study using molecular dynamics simulations

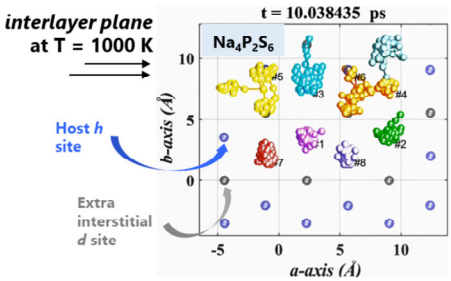

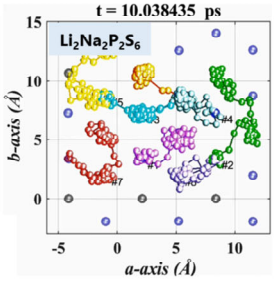

$$C^s_{h\leftrightarrow h}(t) = \begin{cases} C^s_{h\leftrightarrow h}(t-\Delta t) & \text{No config. change} \\ C^s_{h\leftrightarrow h}(t-\Delta t)+1 & h \leftrightarrow \text{nn } h \end{cases}$$

$$C^s_{h\leftrightarrow d}(t) = \begin{cases} C^s_{h\leftrightarrow d}(t-\Delta t) & \text{No config. change} \\ C^s_{h\leftrightarrow d}(t-\Delta t)+1 & \{h,d\} \leftrightarrow \text{nn } \{d,h\} \end{cases}$$

with $C^s_{h\leftrightarrow h}(t=0) = 0 = C^s_{h\leftrightarrow d}(t=0)$.

$$H_{h\leftrightarrow h}(t) = \frac{1}{16}\sum_{s=1}^{16} C^s_{h\leftrightarrow h}(t)$$

$$H_{h\leftrightarrow d}(t) = \frac{1}{16}\sum_{s=1}^{16} C^s_{h\leftrightarrow d}(t).$$

- No g → h and g → g hopping
- All migrations occur within interlayer plane containing h-type Na ions
- Direct h → h vacancy migration is consistent with NEB analysis
- Indirect h → d → h vacancy migration is prevalent
- No interstitial d → d migration

Both Na ion vacancy sites and indirect participation of interstitial sites contribute to the conductivity throughout the interlayer plane

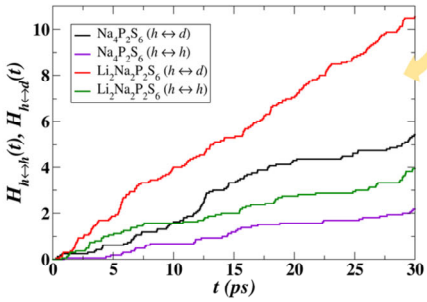

**AIMD simulations were carried out using supercells composed of 2x1x2 conventional units (96 atoms)*

Qualitatively speaking, compared to the case for $Na_4P_2S_6$ the Na ions migrate more frequently in the mixed material $Li_2Na_2P_2S_6$, presenting a more extensive network of diffusional channels. To quantify these effects, we analyzed the nearest-neighbor hopping events, that is, the average number of hops between nearest neighboring sites, as a function of time. The story we can tell from the plots of H vs t is that for each material, the Na ion diffusion is either via direct vacancy mechanism between h to h, or via indirect vacancy mechanism between h to d or d to h. The h to d hops are more prevalent than the h to h hops, suggesting the interstitial d sites play an important role as intermediates in the Na ion migration processes throughout the interlayer plane.

Migration study using molecular dynamics simulations

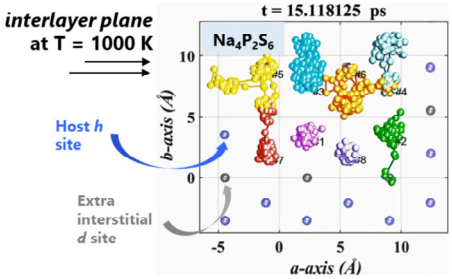

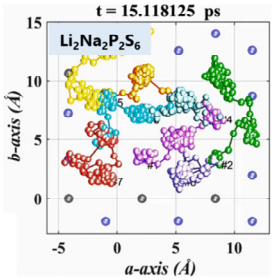

$$C^s_{h\leftrightarrow h}(t) = \begin{cases} C^s_{h\leftrightarrow h}(t-\Delta t) & \text{No config. change} \\ C^s_{h\leftrightarrow h}(t-\Delta t)+1 & h \leftrightarrow \text{nn } h \end{cases}$$

$$C^s_{h\leftrightarrow d}(t) = \begin{cases} C^s_{h\leftrightarrow d}(t-\Delta t) & \text{No config. change} \\ C^s_{h\leftrightarrow d}(t-\Delta t)+1 & \{h,d\} \leftrightarrow \text{nn } \{d,h\} \end{cases}$$

with $C^s_{h\leftrightarrow h}(t=0) = 0 = C^s_{h\leftrightarrow d}(t=0)$.

$$H_{h\leftrightarrow h}(t) = \frac{1}{16}\sum_{s=1}^{16} C^s_{h\leftrightarrow h}(t)$$

$$H_{h\leftrightarrow d}(t) = \frac{1}{16}\sum_{s=1}^{16} C^s_{h\leftrightarrow d}(t).$$

- No g → h and g → g hopping
- All migrations occur within interlayer plane containing h-type Na ions
- Direct h → h vacancy migration is consistent with NEB analysis
- Indirect h → d → h vacancy migration is prevalent
- No interstitial d → d migration

Both Na ion vacancy sites and indirect participation of interstitial sites contribute to the conductivity throughout the interlayer plane

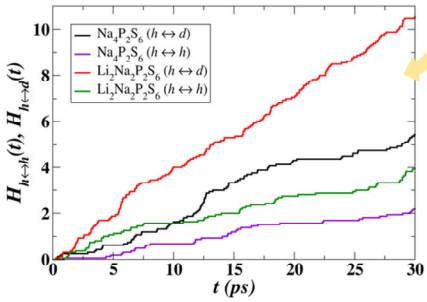

**AIMD simulations were carried out using supercells composed of 2x1x2 conventional units (96 atoms)*

Migration study using molecular dynamics simulations

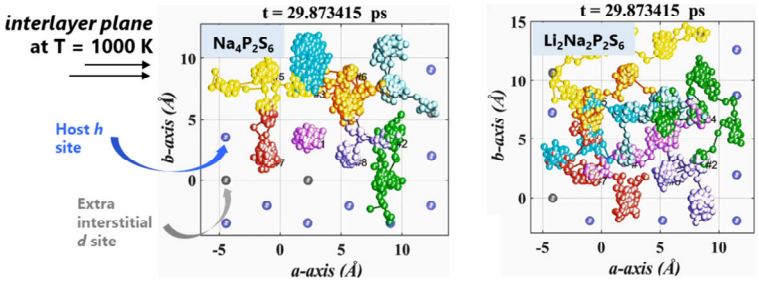

$$C^s_{h\leftrightarrow h}(t) = \begin{cases} C^s_{h\leftrightarrow h}(t-\Delta t) & \text{No config. change} \\ C^s_{h\leftrightarrow h}(t-\Delta t)+1 & h \leftrightarrow \text{nn } h \end{cases}$$

$$C^s_{h\leftrightarrow d}(t) = \begin{cases} C^s_{h\leftrightarrow d}(t-\Delta t) & \text{No config. change} \\ C^s_{h\leftrightarrow d}(t-\Delta t)+1 & \{h,d\} \leftrightarrow \text{nn } \{d,h\} \end{cases}$$

with $C^s_{h\leftrightarrow h}(t=0) = 0 = C^s_{h\leftrightarrow d}(t=0)$.

$$H_{h\leftrightarrow h}(t) = \frac{1}{16}\sum_{s=1}^{16} C^s_{h\leftrightarrow h}(t)$$

$$H_{h\leftrightarrow d}(t) = \frac{1}{16}\sum_{s=1}^{16} C^s_{h\leftrightarrow d}(t).$$

- No g → h and g → g hopping
- All migrations occur within interlayer plane containing h-type Na ions
- Direct h → h vacancy migration is consistent with NEB analysis
- Indirect h → d → h vacancy migration is prevalent
- No interstitial d → d migration

Both Na ion vacancy sites and indirect participation of interstitial sites contribute to the conductivity throughout the interlayer plane

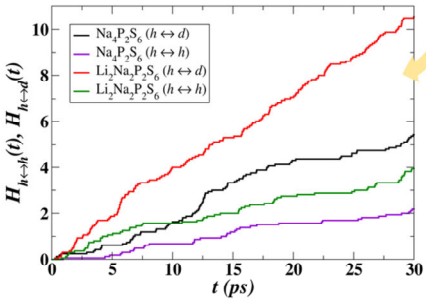

**AIMD simulations were carried out using supercells composed of 2x1x2 conventional units (96 atoms)*

Ionic conductivity (continued)

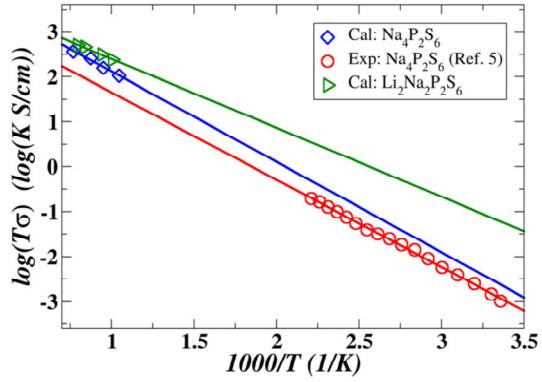

Molecular dynamics analysis of the ionic conductivity. The activation energy is obtained from the slope of the corresponding fit line.

TABLE: NEB and MD results calculated with the PBEsol exchange-correlation functional, in comparison to those of previous work obtained using the LDA exchange-correlation functional and available experimental data. All energies are given in eV units.

Materials	Analysis	E_m	E_f	E_a
$Na_4P_2S_6$	LDA + NEB[1]	0.30	0.24	0.42
	PBEsol + NEB	0.25	0.18	0.34
	PBEsol + MD	--	--	0.41
	Experiment[2]	--	--	0.39
$Li_2Na_2P_2S_6$	PBEsol + NEB	0.16	0.13	0.23
	PBEsol + MD	--	--	0.30

$Li_2Na_2P_2S_6$ presents better Na ion conductivity than $Na_4P_2S_6$

[1]Rush et al., *Solid State Phys.* **286**, 45-50 (2016)
[2]Hood et al., Manuscript in preparation.

Both NEB and molecular dynamics analyses suggest that the mixed ion material $Li_2Na_2P_2S_6$ has lower activation barriers and larger conductivity compared with $Na_4P_2S_6$. The present computational results on $Na_4P_2S_6$ are in reasonable agreement with the available calculated results using LDA in Ref. 1 and the experimental measurement in Ref. 2.

We also noticed that for these systems, $E_a^{NEB} \neq E_a^{MD}$ because of their different treatments of the effects of interstitial d sites. The NEB analysis presented here only considered direct hops between nearest neighbor vacancy sites, including the interstitial sites only in the estimation of the population of vacancies via the Boltzmann factor due to the formation energy E_f of the interstitial-vacancy pair. The molecular dynamics results indicate significant contributions of hops between vacancy and interstitial sites, presenting a plausibly more physical picture of the Na ion migration processes.

Summary

- Using first-principle computational tools, we predicted the structure of a possible mixed ion material $Li_2Na_2P_2S_6$ and analyzed its stability in terms of Helmholtz free energies of proposed reaction pathways.
- Conductivity studies on both $Na_4P_2S_6$ and $Li_2Na_2P_2S_6$ indicates that Na ions move primarily within the interlayer region between the $(P_2S_6)^{4-}$ layers, efficiently proceeding via direct or indirect hops between vacancy sites, with indirect processes involving intermediate interstitial sites.
- $Li_2Na_2P_2S_6$ has larger conductivity and lower activation barriers compared with $Na_4P_2S_6$, suggesting that the predicted material to be more promising Na ion electrolytes.